IOP Publishing Bioinspiration & Biomimetics
Bioinspir. Biomim. **9** (2014) 016002 (13pp) doi:10.1088/1748-3182/9/1/016002

Kinematic feedback control laws for generating natural arm movements

Donghyun Kim, Cheongjae Jang and Frank C Park[1]

School of Mechanical and Aerospace Engineering, Seoul National University, Seoul 151-744, Korea

E-mail: fcp@snu.ac.kr

Received 22 July 2013
Accepted for publication 5 November 2013
Published 16 December 2013

Abstract

We propose a stochastic optimal feedback control law for generating natural robot arm motions. Our approach, inspired by the minimum variance principle of Harris and Wolpert (1998 *Nature* **394** 780–4) and the optimal feedback control principles put forth by Todorov and Jordan (2002 *Nature Neurosci.* **5** 1226–35) for explaining human movements, differs in two crucial respects: (i) the endpoint variance is minimized in joint space rather than Cartesian hand space, and (ii) we ignore the dynamics and instead consider only the second-order differential kinematics. The feedback control law generating the motions can be straightforwardly obtained by backward integration of a set of ordinary differential equations; these equations are obtained exactly, without any linear–quadratic approximations. The only parameters to be determined *a priori* are the variance scale factors, and for both the two-DOF planar arm and the seven-DOF spatial arm, a table of values is constructed based on the given initial and final arm configurations; these values are determined via an optimal fitting procedure, and consistent with existing findings about neuromuscular motor noise levels of human arm muscles. Experiments conducted with a two-link planar arm and a seven-DOF spatial arm verify that the trajectories generated by our feedback control law closely resemble human arm motions, in the sense of producing nearly straight-line hand trajectories, having bell-shaped velocity profiles, and satisfying Fitts Law.

(Some figures may appear in colour only in the online journal)

1. Introduction

In the case of robots operating in human environments and intended to interact with humans, for various reasons it is usually desirable to have the robot's motions resemble human movements. The existing literature on human-like robot motion generation is focused for the most part on finding ways for the robot to imitate human motions: given a set of human motion sequences obtained via, e.g., motion capture data, such sequences are then used as training sets for a learning algorithm, which typically extracts a set of movement primitives—for example, a basis of motion trajectories obtained via principal component analysis of the training data—that are then used to interpolate more general robot motions (Pollard *et al* 2002, Arikan and Forsyth 2002, Ren *et al* 2005, Lim *et al* 2005, Harada *et al* 2006, Yamane *et al* 2010). Because the human and robot typically have different dimensions and topologies, finding appropriate ways to map human motions to the robot have dominated this line of investigation. Numerous variations on this theme have been proposed, but the end result in most cases is a motion trajectory parametrized with respect to time.

While for animation purposes a time-parametrized motion trajectory may be sufficient, in robotics a control law, preferably in feedback form, is generally much more useful. Among other things, a feedback control law is far more robust to noise and modeling errors than any open-loop control. In principle one could supply the motion trajectory as a reference trajectory to a tracking controller, which likely uses feedback to correct for small tracking errors. Generating the motion trajectory, however, not only requires substantive computational effort, but is also subject to modeling errors.

Such practical difficulties explain to some extent the popularity of artificial potential field-based methods for robot

[1] Author to whom any correspondence should be addressed.

planning and control (Khatib 1986); these lead to purely feedback control-based realizations for generating feasible motions, that also have the effect of blurring the traditional distinction between planning (in the sense of generating a reference trajectory) and control (in the sense of tracking a reference trajectory). Of course, the choice of potential function defines the nature of the motion, and finding a potential function that generates natural motions remains elusive.

The question of what constitutes a natural motion, or more fundamentally, how humans generate movements, is of course the central question in human motor control. While universal principles are not easy to come by, it is by now generally agreed that, at least for simple point-to-point arm motions, there are certain features shared by nearly all humans:

(i) the hand traces nearly a straight line;
(ii) the hand speed profile is bell-shaped;
(iii) the motions satisfy Fitts Law (Fitts 1954), which relates a movement's duration to its difficulty according to

$$T \propto \log_2\left(\frac{2A}{W}\right), \tag{1}$$

where T denotes the movement duration, A the distance between the hand's start and goal configurations, and W is the target width.

These observations serve as a useful benchmark for evaluating various principles that attempt to explain human arm movements. Of the many hypotheses on human movement, the equilibrium point hypothesis (see Feldman 1966, Flash 1987, Shadmehr 1998 and the references cited therein) and the minimum variance hypothesis (Harris and Wolpert 1998) have been particularly relevant from the perspective of robotics. Loosely speaking, the former postulates that human muscles function as pairs of antagonistic springs, and that humans generate movements by shifting their equilibrium lengths. While questions linger about how accurately the equilibrium point hypothesis explains human movements (see, e.g., Hinder and Milner 2003), this is an attractive concept for robot control that is in many respects consistent with the artificial potential field-based approach to motion generation and control—without necessarily resorting to complex internal dynamics calculations, motions are generated simply by application of a feedback control law. The difficulty, and a crucial one at that, is that the equilibrium point hypothesis in itself does not suggest any specific potential field that leads to natural, human-like robot motions.

The minimum variance hypothesis (Harris and Wolpert 1998) takes the point of view that motor control signals are corrupted by noise whose variance is proportional to the signal amplitude—this explains, among other things, the observed variations in repeated trials of a motion performed by a person—and that the human motor control system generates motions that attempt to minimize the position variance at the target. The experimental evidence presented in Harris and Wolpert (1998) makes a compelling case for the minimum variance hypothesis, with predicted motions satisfying the characteristic features of human arm movements.

One of the challenges in applying the minimum variance principle to generate robot motions is that the solution of a nonlinear stochastic optimal control problem is required. Not only is this computationally challenging (assuming that a solution even exists), but typically the solutions are obtained in the form of time trajectories rather than the desired feedback control law form. In Simmons and Demiris (2005) a discrete-time linear–quadratic regulator implementation of a minimum variance controller is presented, but this formulation ignores both the inherent nonlinearities in the problem and the proper rules for stochastic calculus; as is well-known, the calculus for systems driven by Brownian motion is fundamentally different from the rules for ordinary calculus. In Todorov and Jordan (2002) a highly compelling case is made for optimal stochastic feedback control as a framework for explaining human movements. Even here, however, the intractability of finding solutions in the general nonlinear case is recognized, and only linear–quadratic Gaussian approximation techniques are developed.

In this paper we present, as our main contribution, a robot feedback control law based on the minimum variance hypothesis. Unlike (Harris and Wolpert 1998), which considers the dynamics, our formulation is based on a continuous-time, second-order differential equation formulation of the robot's kinematics. This is an important advantage when considering that most commercially available humanoid robots today allow for only kinematic (position, and depending on the accuracy of the joint encoders, velocity and acceleration) control; very few humanoid robots allow for direct joint torque control. Our method also correctly accounts for the signal-dependent noise process by following the rules for stochastic (Itō) calculus.

A second point of departure from the original minimum variance hypothesis of Harris and Wolpert (1998) is that we minimize the endpoint variance in joint space rather than Cartesian hand space. This entails the adjustment of scale factors for the variance of the input signal noise depending on the target location. In the case of planar two-link arm motions we show that there is in fact a neuromuscular basis for choosing these values *a priori*; for more general seven degree of freedom arms, the choice of variance scale factors seems to have minimal effect on the resulting arm motions. As a result of formulating the problem entirely in joint space, our optimal feedback control law is obtained in analytic form by exactly solving the Hamilton–Jacobi–Bellman (HJB) equations. The optimal time-varying gains can be obtained by integrating a set of simple first-order ordinary differential equations, analogous to solving the matrix Riccati equations in the classical linear–quadratic Gaussian control framework. Unlike existing approaches, our method involves no linear–quadratic approximations.

Despite these two variations from the original minimum variance hypothesis—ignoring the dynamics and considering only the kinematics in the state equations, and formulating the endpoint variance in joint space—extensive numerical experiments with our feedback control law confirm that the resulting motions are indeed quite human-like with respect to the criteria described earlier; for both a two-link planar open chain and a spatial seven degree-of-freedom arm, we find that

the resulting motions closely match those of typical human arm motions.

The paper is organized as follows. In section 2 we first present some essential background on stochastic optimal control, followed by a derivation of our optimal feedback control law for a two-link planar chain, and its extension to general n-link spatial open chains. Numerical experiments comparing the generated motions with human arm movements are presented in section 4. We conclude in section 5 with a summary and some discussion of the possible broader implications of our results to human motor control.

2. Optimal feedback control law

2.1. Stochastic optimal control preliminaries

We consider the stochastic optimal control problem in a continuous time setting. The state dynamics is of the form

$$\mathrm{d}q = f(t, q, u)\,\mathrm{d}t + g(t, q, u)\,\mathrm{d}\omega, \tag{2}$$

where $q \in \mathbb{R}^n$ is the state, $u \in \mathbb{R}^p$ is the input control, $\mathrm{d}\omega \in \mathbb{R}^m$ denotes a vector of m independent Wiener processes interpreted in the Itō sense, and the mappings $f : \mathbb{R} \times \mathbb{R}^n \times \mathbb{R}^p \to \mathbb{R}^n$ and $g : \mathbb{R} \times \mathbb{R}^n \times \mathbb{R}^p \to \mathbb{R}^{n\times m}$ are right-continuous in t and uniformly Lipschitz continuous in (q, u). We assume the initial state $q(t_0)$ is given. The objective is to find u that minimizes the terminal cost

$$\inf_u E[\phi(t_f, q(t_f))], \tag{3}$$

where $E[\cdot]$ denotes expectation. The optimal cost-to-go function V is defined as follows:

$$V(s, q) = \inf_u E[\phi(t_f, q(t_f))]. \tag{4}$$

Any twice-differentiable $V(t, q)$ that is optimal must necessarily satisfy the following HJB equation:

$$-V_t(t, q) = +\inf_u \left[V_q(t, q, u) f(t, q, u) + \frac{1}{2}\mathrm{tr}(V_{qq}(t, q) g(t, q, u) g(t, q, u)^T) \right], \tag{5}$$

where subscripts denote partial differentiation, e.g., V_t denotes the partial derivative of V with respect to t, and V_q and V_{qq} are given by

$$V_q = \begin{bmatrix} V_{q_1} & \cdots & V_{q_n} \end{bmatrix} \in \mathbb{R}^{1\times n} \tag{6}$$

$$V_{qq} = \begin{bmatrix} V_{q_1q_1} & \cdots & V_{q_1q_n} \\ \vdots & \ddots & \vdots \\ V_{q_nq_1} & \cdots & V_{q_nq_n} \end{bmatrix} \in \mathbb{R}^{n\times n}. \tag{7}$$

The corresponding boundary conditions for the HJB equation are

$$V(t_f, q(t_f)) = \phi(t_f, q(t_f)). \tag{8}$$

Stochastic optimal control problems in which the objective function contains an integral term, i.e.,

$$\inf_u E\left[\phi(t_f, q(t_f)) + \int_0^{t_f} L(t, q, u)\,\mathrm{d}t \right], \tag{9}$$

where $L \in \mathbb{R}$ is differentiable in (t, q, u), can be transformed to the earlier form by introducing a new state variable $q_0(t) = \int_0^t L(s, q, u)\mathrm{d}s$; the equation $\mathrm{d}q_0 = L(t, q, u)\mathrm{d}t$ is then augmented to the original state equations, and the objective function (9) can now be expressed as

$$\inf_u E[\phi(t_f, q(t_f)) + q_0(t_f)] \tag{10}$$

which is of the same form as (3). Further basic results on stochastic optimal control can be found in, e.g., Seierstad (2008).

2.2. Planar two-link open chain

We now consider a planar two-link open chain consisting of two revolute joints, which has been widely used to model human arms performing planar reaching tasks. Following (Harris and Wolpert 1998), we assume signal-dependent noise enters into the second-order kinematics of the chain as follows. Denoting the revolute joint angles by (θ_1, θ_2), the state $q \in \mathbb{R}^4$ is defined according to $q_1 = \theta_1, q_2 = \theta_2, q_3 = \dot\theta_1$, and $q_4 = \dot\theta_2$. The state equations are given by

$$d\begin{bmatrix} q_1 \\ q_2 \\ q_3 \\ q_4 \end{bmatrix} = \begin{bmatrix} q_3 \\ q_4 \\ u_1 \\ u_2 \end{bmatrix} \mathrm{d}t + \begin{bmatrix} 0 & 0 \\ 0 & 0 \\ \sqrt{\sigma_1}|u_1| & 0 \\ 0 & \sqrt{\sigma_2}|u_2| \end{bmatrix} \begin{bmatrix} \mathrm{d}w_1 \\ \mathrm{d}w_2 \end{bmatrix}, \tag{11}$$

where u_1, u_2 denote the input joint accelerations, $\mathrm{d}w_1$, $\mathrm{d}w_2$ are independent Wiener processes, and σ_1, σ_2 are positive constants corresponding to the noise variance. Observe that the noise terms in the state equations are scaled by the input signal strengths $|u_1|$ and $|u_2|$.

In this paper we consider the objective function given by

$$\inf_u E[(q(t_f) - \bar q)^T D(q(t_f) - \bar q)], \tag{12}$$

where $\bar q = (\bar\theta_1, \bar\theta_2, \dot{\bar\theta}_1, \dot{\bar\theta}_2)$ denotes the desired final state and $D = \mathrm{Diag}\{d_1, \ldots, d_4\}$ is an arbitrary positive definite diagonal matrix. The corresponding HJB equations are

$$-V_t = \inf_u \left[V_1q_3 + V_2q_4 + V_3u_1 + V_4u_2 + \frac{1}{2}\sigma_1V_{33}u_1^2 + \frac{1}{2}\sigma_2V_{44}u_2^2 \right], \tag{13}$$

where we use the shorthand notation $V_i = \frac{\partial V}{\partial q_i}$, $V_{ij} = \frac{\partial^2 V}{\partial q_i \partial q_j}$. The Hamiltonian is given by

$$H = V_1q_3 + V_2q_4 + V_3u_1 + V_4u_2 + \tfrac{1}{2}\sigma_1V_{33}{u_1}^2 + \tfrac{1}{2}\sigma_2V_{44}{u_2}^2. \tag{14}$$

Since no constraints are imposed on u, the necessary conditions $\frac{\partial H}{\partial u_i} = 0$, $i = 1, 2$, can be applied to derive the optimal form of the u_i^*:

$$u_1^* = -\frac{V_3}{\sigma_1V_{33}}, \quad u_2^* = -\frac{V_4}{\sigma_2V_{44}}. \tag{15}$$

Substituting the above into the HJB equations (13) leads to

$$-V_t = \inf_u \left[V_1q_3 + V_2q_4 - \frac{1}{2\sigma_1}\frac{V_3^2}{V_{33}} - \frac{1}{2\sigma_2}\frac{V_4^2}{V_{44}} \right]. \tag{16}$$

Taking into account the quadratic cost function, we assume the following form for V:

$$V(t,q) = k_1 q_1^2 + k_2 q_2^2 + k_3 q_3^2 + k_4 q_4^2 + k_5 q_1 + k_6 q_2 + k_7 q_3 + k_8 q_4 + k_9 q_1 q_3 + k_{10} q_2 q_4 + k_{11}, \quad (17)$$

where only the $k_i(t)$ depend explicitly on t. The optimal u_i^* of equation (15) then becomes

$$u_1^* = -\frac{2k_3 q_3 + k_7 + k_9 q_1}{2\sigma_1 k_3} \quad (18)$$

$$u_2^* = -\frac{2k_4 q_4 + k_8 + k_{10} q_2}{2\sigma_2 k_4}. \quad (19)$$

Substituting (17) into the HJB equations (16) and matching terms on both sides then leads to the following set of eleven ordinary differential equations:

$$\begin{aligned}
&\dot{k}_1 = \frac{k_9^2}{4\sigma_1 k_3} && \dot{k}_2 = \frac{k_{10}^2}{4\sigma_2 k_4}\\
&\dot{k}_3 = -k_9 + \frac{k_3}{\sigma_1} && \dot{k}_4 = -k_{10} + \frac{k_4}{\sigma_2}\\
&\dot{k}_5 = \frac{k_7 k_9}{2\sigma_1 k_3} && \dot{k}_6 = \frac{k_8 k_{10}}{2\sigma_2 k_4}\\
&\dot{k}_7 = -k_5 + \frac{k_7}{\sigma_1} && \dot{k}_8 = -k_6 + \frac{k_8}{\sigma_2}\\
&\dot{k}_9 = -2k_1 + \frac{k_9}{\sigma_1} && \dot{k}_{10} = -2k_2 + \frac{k_{10}}{\sigma_2} \qquad \dot{k}_{11} = \frac{k_7^2}{4\sigma_1 k_3} + \frac{k_8^2}{4\sigma_2 k_4}
\end{aligned} \quad (20)$$

subject to the following set of terminal boundary conditions at t_f:

$$\begin{aligned}
&k_i(t_f) = d_i, \ i = 1, \ldots, 4,\\
&k_5(t_f) = -2d_1\bar{q}_1, \quad k_6(t_f) = -2d_2\bar{q}_2,\\
&k_7(t_f) = -2d_3\dot{\bar{q}}_1, \quad k_8(t_f) = -2d_4\dot{\bar{q}}_2\\
&k_9(t_f) = k_{10}(t_f) = 0, \quad k_{11}(t_f) = \bar{q}^T D \bar{q}.
\end{aligned} \quad (21)$$

Moreover, if the final joint velocities $\dot{\bar{q}}_1$ and $\dot{\bar{q}}_2$ are both zero, the feedback gains k_5, k_6, k_7, and k_8 can then be expressed as

$$\begin{aligned}
&k_5 = -2k_1\bar{q}_1 - k_9\bar{q}_3, \quad k_6 = -2k_2\bar{q}_2 - k_{10}\bar{q}_4,\\
&k_7 = -k_9\bar{q}_1 - 2k_3\bar{q}_3, \quad k_8 = -k_{10}\bar{q}_2 - 2k_4\bar{q}_4.
\end{aligned} \quad (22)$$

(Note: The above can be verified by defining the variables $c = k_5 + 2k_1\bar{q}_1 + k_9\bar{q}_3$ and $d = k_7 + k_9\bar{q}_1 + 2k_3\bar{q}_3$, in which case

$$\frac{\mathrm{d}}{\mathrm{d}t}\begin{bmatrix} c \\ d \end{bmatrix} = \begin{bmatrix} 0 & \frac{k_9}{2\sigma_1 k_3} \\ -1 & \frac{1}{\sigma_1} \end{bmatrix}\begin{bmatrix} c \\ d \end{bmatrix} + \begin{bmatrix} -2k_1 \\ -k_9 \end{bmatrix}\bar{q}_3 \quad (23)$$

follows from (20). Since $\dot{\bar{q}}_1 = \bar{q}_3 = 0$ and $c(t_f) = d(t_f) = 0$ follows from the boundary conditions (21), backward integration of the above differential equation leads to $c(t) = d(t) = 0$, and equation (22) holds over the interval $t \in [0, t_f]$. Analogous results for (k_6, k_8) also hold by the same line of reasoning). Also from (18) and (19), the optimal u_i^* can be expressed in the following more intuitive form:

$$u_1^* = -\frac{2k_3 q_3 + k_7 + k_9 q_1}{2\sigma_1 k_3} = -\frac{k_9(q_1 - \bar{q}_1) + 2k_3(q_3 - \bar{q}_3)}{2\sigma_1 k_3} \quad (24)$$

$$u_2^* = -\frac{2k_4 q_4 + k_8 + k_{10} q_2}{2\sigma_2 k_4} = -\frac{k_{10}(q_2 - \bar{q}_2) + 2k_4(q_4 - \bar{q}_4)}{2\sigma_2 k_4}. \quad (25)$$

Note that because k_3 and k_4 appear in the denominators of some of the differential equations and optimal inputs above, we need to examine under what conditions, if any, k_3 and k_4 become zero during the duration of the motion. The following proposition shows that this can never occur.

Proposition 1. *The solutions $k_i(t)$, $i = 1, \ldots, 11$ to the differential equations above are all finite-valued and continuous over the interval $t \in [0, t_f]$.*

Proof. Observing that the equation for k_3 is coupled only with those for k_1 and k_9, we examine the differential equations for (k_1, k_3, k_9) more closely; the equations for (k_2, k_4, k_{10}) are structurally identical. Without loss of generality we assume the diagonal matrix D is the identity. Letting $x = k_1$, $y = k_3$, $z = k_9$, and $c = \sigma_1$, we have

$$\begin{aligned}
\dot{x} &= \frac{z^2}{4cy}\\
\dot{y} &= -z + \frac{y}{c}\\
\dot{z} &= -2x + \frac{z}{c},
\end{aligned}$$

with boundary conditions $x(t_f) = y(t_f) = 1$ and $z(t_f) = 0$. Since the boundary conditions are given at t_f—the equations need to be integrated backward in time—we make the substitution $t \leftarrow t_f - t$ and examine the reverse flow; we therefore consider the following differential equations with respect to this newly defined t:

$$\dot{x} = -\frac{z^2}{4cy} \quad (26)$$

$$\dot{y} = z - \frac{y}{c} \quad (27)$$

$$\dot{z} = 2x - \frac{z}{c}, \quad (28)$$

with initial boundary conditions $x(0) = y(0) = 1$ and $z(0) = 0$. It is enough to show that a solution $(x(t), y(t), z(t))$ exists for all $t \geqslant 0$ and further satisfies $y(t) > 0$. For this purpose consider the function $V(x, y, z) = xy - \frac{1}{4}z^2$. Taking the time derivative of V along the solution $(x(t), y(t), z(t))$,

$$\begin{aligned}
\dot{V} &= \dot{x}y + x\dot{y} - \frac{1}{2}z\dot{z}\\
&= -\frac{1}{c}\left(xy - \frac{z^2}{4}\right)\\
&= -\frac{V}{c},
\end{aligned}$$

whose solution is given by $V(t) = \mathrm{e}^{-t/c}V(0) = \mathrm{e}^{-t/c}$. Therefore along a solution trajectory we have

$$V(x(t), y(t), z(t)) = \mathrm{e}^{-t/c} = x(t)y(t) - \tfrac{1}{4}z(t)^2, \quad (29)$$

or

$$x(t)y(t) = \tfrac{1}{4}z(t)^2 + \mathrm{e}^{-t/c} > 0.$$

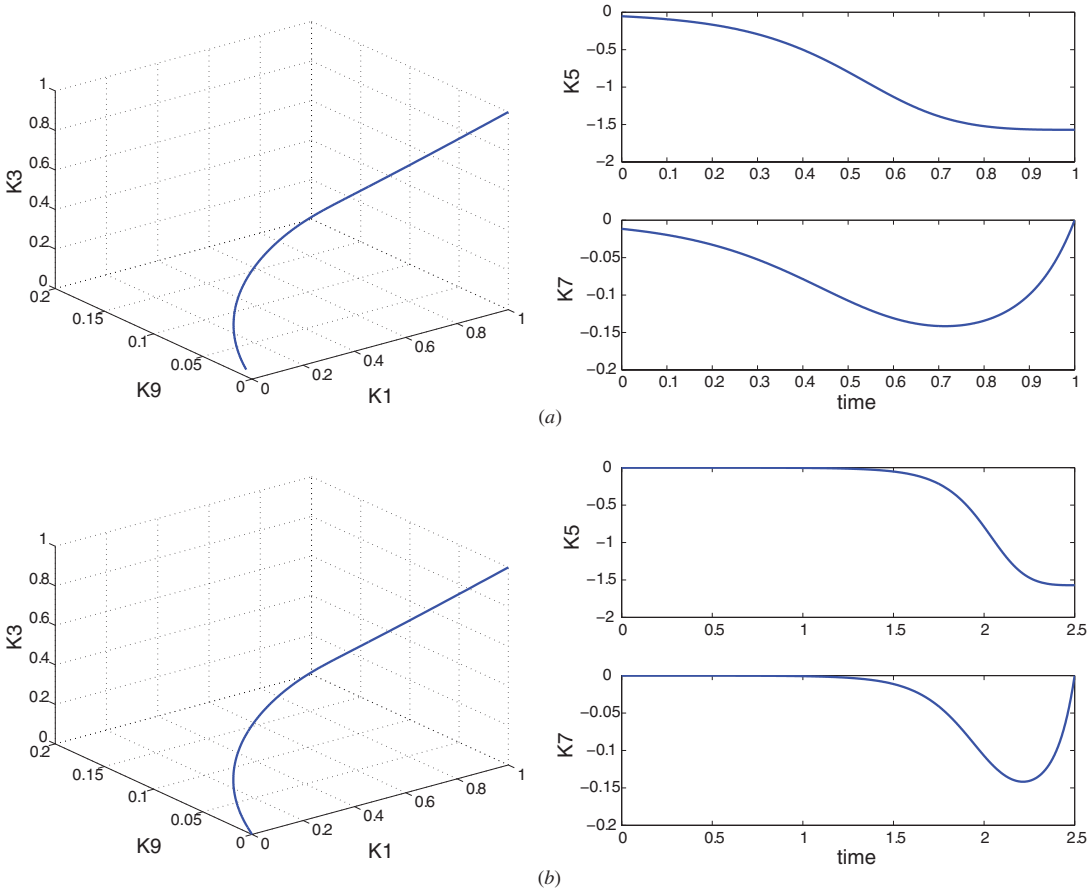

Figure 1. Feedback gain trajectories for different movement durations. (*a*) Movement time = 1.0 s. (*b*) Movement time = 2.5 s.

Since both $x(0)$ and $y(0)$ are positive, it follows that both $x(t)$ and $y(t)$ remain positive for all $t \geqslant 0$. In fact, as t approaches infinity, from equation (29) it can be seen that z^2 approaches $4xy$; in the limit the differential equation (26) becomes $\dot{x} = -x/c$, whose solution $x(t)$ clearly approaches zero as t goes to infinity. It thus follows from (28) that $z(t)$ goes to zero as t approaches infinity; this in turn implies, from (27), that $y(t)$ also goes to zero in the limit. Thus, the solution trajectory $(x(t), y(t), z(t))$ originating from $(1, 1, 0)$ at $t = 0$ approaches zero in the limit, with $x(t), y(t) > 0$ for all t. This in turn implies that both $k_3(t)$ and $k_4(t)$ remain positive for all $t \in (-\infty, t_f]$. The other $k_i(t)$ are therefore all well-defined (finite-valued and continuous) over the interval $[0, t_f]$. □

Backward numerical integration of the differential equations in $\{k_1(t), \ldots, k_{11}(t)\}$ also confirms the above result. Figure 1 plots time profiles of $k_1(t)$, $k_3(t)$, $k_5(t)$, $k_7(t)$, and $k_9(t)$ for $t_f = 1.0$ s and $t_f = 2.5$ s, respectively, and c set to 1. Since typical arm reaching movements take on the order of 1–2 s at most, we see that the gains are bounded and well-behaved for finite duration movements.

2.3. Comparison with Harris and Wolpert's formulation

In the original minimum variance formulation proposed in Harris and Wolpert (1998), the cost function is defined in Cartesian hand space rather than joint space, and the dynamic equations are taken to be the state equations. Specifically, with $\theta = (\theta_1, \theta_2)$ denoting the joint variables, the dynamic equations are of the form

$$u = M(\theta)\ddot{\theta} + b(\theta, \dot{\theta}), \tag{30}$$

where $u \in \mathbb{R}^2$ denotes the vector of input joint torques, $M(\theta) \in \mathbb{R}^{2\times 2}$ is the mass matrix, and $b(\theta, \dot{\theta}) \in \mathbb{R}^2$ is a two-dimensional bias torque vector. The end-effector Cartesian coordinates (x, y) are determined from (θ_1, θ_2) via the forward kinematics:

$$x = l_1 \cos\theta_1 + l_2 \cos(\theta_1 + \theta_2) \tag{31}$$

$$y = l_1 \sin\theta_1 + l_2 \sin(\theta_1 + \theta_2), \tag{32}$$

where l_1, l_2 denote the link lengths. As before, defining $q_1 = \theta_1$, $q_2 = \theta_2$, $q_3 = \dot{\theta}_1$, $q_4 = \dot{\theta}_2$, the state equations are then of the form

$$\mathrm{d}q_1 = q_3\,\mathrm{d}t \tag{33}$$

$$\mathrm{d}q_2 = q_4\,\mathrm{d}t \tag{34}$$

$$d\begin{bmatrix} q_3 \\ q_4 \end{bmatrix} = M^{-1}\,(u - b)\;\mathrm{d}t + \begin{bmatrix} |u_1|\,\mathrm{d}w_1 \\ |u_2|\,\mathrm{d}w_2 \end{bmatrix}. \tag{35}$$

The cost function associated with the minimum variance criterion is given by

$$\inf_{u} \int_{t_f}^{t_f+t_s} \mathrm{Var}[x(s)] + \mathrm{Var}[y(s)]\,\mathrm{d}s, \tag{36}$$

where t_s is a fixed post-movement settling time, $\mathrm{Var}[x] = E[x^2] - E^2[x]$, and $\mathrm{Var}[y] = E[y^2] - E^2[y]$. Since $E[x]$ and $E[y]$ are assumed fixed to some known desired values over the interval $[t_f, t_f + t_s]$, the integrand of the cost function (ignoring the constant $E^2[x]$ and $E^2[y]$ terms) simplifies to

$$E[x^2] + E[y^2] = E[l_1^2 + l_2^2 + 2l_1 l_2 \cos q_2]. \tag{37}$$

It is interesting to observe that the cost function depends on q_2 alone; there is no dependence on q_1. Moreover, both the mass matrix M and the bias torque vector b for the two-link planar chain also depend only on q_2. The situation is much the same even for general n-link planar chains; that is, q_1 does not appear explicitly either in the cost function or the dynamics, since $E[x^2+y^2]$ is the squared length from the origin to the end-effector and obviously depends only on the value of $q_2 = \theta_2$.

The problem as formulated is highly nonlinear and does not lead to analytic solutions; in fact, little if anything can be said about even the existence of solutions. For this reason (Harris and Wolpert 1998), and other works like (Simmons and Demiris 2005, Todorov and Jordan 2002), implement a linear–quadratic approximation to the minimum variance model.

2.4. Choosing variance scale factors

In the two-link planar arm formulation, observe that the variance scale factors σ_1 and σ_2 enter into the feedback gain equations (20), and thus influence the resulting optimal arm motion. Larger values of σ_1 and σ_2 produce larger input noise, and can be identified with the neuromuscular motor noise levels corresponding to the relevant muscles. In Gabriel (1997), an attempt is made to experimentally measure neuromuscular signal levels associated with the major arm muscles. Among its findings, it is suggested that for normal speed arm motions involving the elbow, the triceps brachii has a greater associated noise variance than the biceps brachii. The biceps and triceps brachii act as an agonist-antagonist pair during elbow flexion, and conversely as an antagonist-agonist pair during elbow extension. Since for typical motions the agonist muscle is the dominant muscle, one would expect the noise variance to be larger for arm motions that involve elbow extensions.

Of course, the robot arms that we consider in this paper are actuated not by muscles, but by rotary actuators that drive the joints. Hence, in the case of the planar arm, to apply larger input signal noise levels for elbow extensions rather than flexions requires that the relative values of σ_1 and σ_2 not be assumed constant, but rather allowed to vary according to the start and goal arm postures.

Toward this end, we perform numerical experiments to find values for σ_1 and σ_2 that lead to natural arm movements, and determine if they are consistent with our intuitive reasoning about input noise levels outlined earlier. We consider a two-link planar arm with equal link lengths $L_1 = L_2 = 0.35$ m, at a range of initial postures defined by

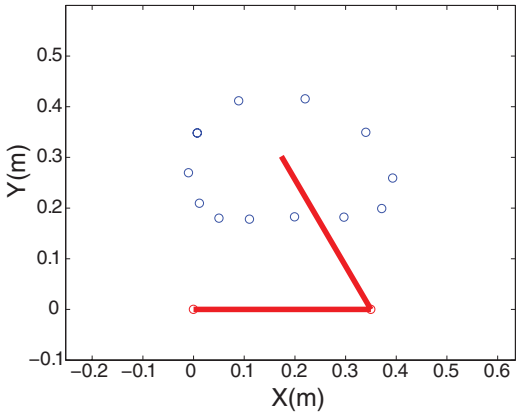

Figure 2. Two-link planar arm used in variance scale factor determination experiments. Blue circles represent some of the goal postures in task space.

$q_1 = 0.0$ radians and $q_2 \in [0.6, 2.6]$ radians (figure 2 shows the chain at the initial posture $q_1 = 0$, $q_2 = 2.1$). The goal postures are taken to be a set of equally spaced points on the circle in q_1-q_2 space, centered at the initial posture, with a radius 0.5 radians. The total movement duration for each goal posture is set to 0.8 s. For all goal postures we then attempt to determine the values of σ_1 and σ_2 in the range $[0, 0.5]$ that produce the most natural arm movements, by solving a set of optimization problems. From the features of point-to-point arm motions (the hand traces a nearly linear path, velocity profiles are bell-shaped, etc), we now minimize a weighted objective function of the form

$$J = w_1 J_{\mathrm{traj}} + w_2 J_{\mathrm{vel}},$$

where $J_{\mathrm{traj}} = \int_{\mathcal{D}} \mathrm{d}A$ is the area of the task space region enclosed by the generated trajectory and a straight line connecting the start and goal points, and

$$J_{\mathrm{vel}} = \left(t_{\mathrm{peak}} - \frac{t_f}{2}\right)^2$$

measures the deviation from a bell-shaped velocity profile (t_{peak} denotes the time at which the hand tip velocity reaches a maximum). The weights w_1 and w_2 are set so that J_{traj} and J_{vel} are of similar magnitude for the trajectories generated by our controller.

The results of the optimization are shown in the polar plot of figure 3. The origin indicates the initial posture $q_1(0) = 0$, $q_2(0) \in [0.6, 2.6]$. For each initial posture, and each heading direction emanating radially from the origin, the optimal values for σ_1 and σ_2 are plotted in the figure; these are indicated by the black (σ_1) and gray (σ_2) regions, respectively. Note especially the discontinuities that occur when the heading angle θ equals 0, $\pi/2$, π, and $3\pi/2$. These can be explained by examination of equations (24) and (25) for the optimal u_i^*, which we repeat here:

$$u_1^* = -\frac{k_9(q_1 - \bar{q}_1) + 2k_3(q_3 - \bar{q}_3)}{2\sigma_1 k_3}$$
$$u_2^* = -\frac{k_{10}(q_2 - \bar{q}_2) + 2k_4(q_4 - \bar{q}_4)}{2\sigma_2 k_4}.$$

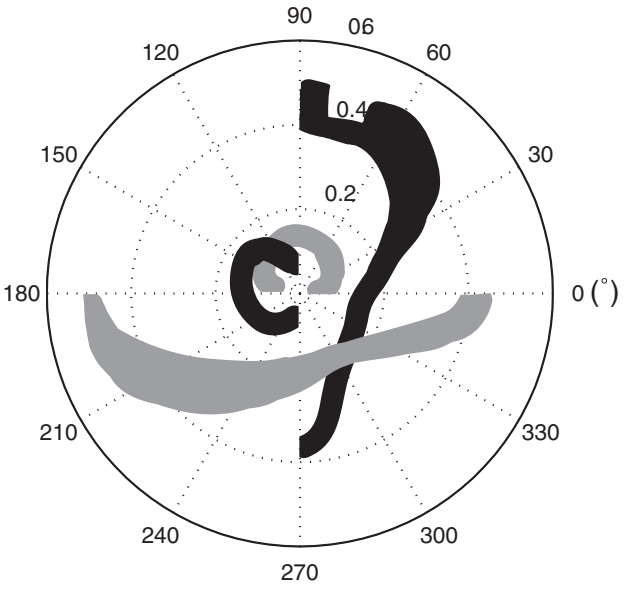

Figure 3. Experimental results for determining variance scale factors. Values for σ_1 and σ_2 are indicated in black and gray, respectively.

Suppose the initial and final joint configurations are $(q_1(0), q_2(0))$ and $(\bar{q}_1, \bar{q}_2)$, respectively. If the desired heading angle is given by $\theta = 0$, this implies that $\bar{q}_2 = q_2(0)$. From the above equations for the optimal feedback control it can be seen that

$$u_1^* = -\frac{k_9(q_1 - \bar{q}_1) + 2k_3(q_3 - \bar{q}_3)}{2\sigma_1 k_3}$$
$$u_2^* = 0.$$

Since $u_2^* = 0$, only σ_1 enters into the input control; the relative value of σ_2 has no effect on the optimal arm motion when $\theta = 0$. The discontinuities that occur at $\theta = \pi/2, \pi, 3\pi/2$ can also be explained similarly.

We also observe that the results of figure 3 vary only slightly for different kinematic parameters and movement durations. The choice of variance parameters for spatial n-link open chains is addressed in the next section.

3. Spatial open chains

The two-DOF planar open chain results can be straightforwardly extended to general n-DOF spatial open chains. Denoting the joint angles by $(\theta_1, \ldots, \theta_n)$, the state $q \in \mathbb{R}^{2n}$ is given by

$$\begin{bmatrix} q_1 & \cdots & q_n & q_{n+1} & \cdots & q_{2n} \end{bmatrix} = \begin{bmatrix} \theta_1 & \cdots & \theta_n & \dot{\theta}_1 & \cdots & \dot{\theta}_n \end{bmatrix}. \quad (38)$$

The state equations are

$$d\begin{bmatrix} q_i \\ q_{n+i} \end{bmatrix} = \begin{bmatrix} q_{n+i} \\ u_i \end{bmatrix} \mathrm{d}t + \begin{bmatrix} 0 \\ \sqrt{\sigma_i}|u_i| \end{bmatrix} \mathrm{d}\omega_i, \quad i = 1, \ldots, n. \quad (39)$$

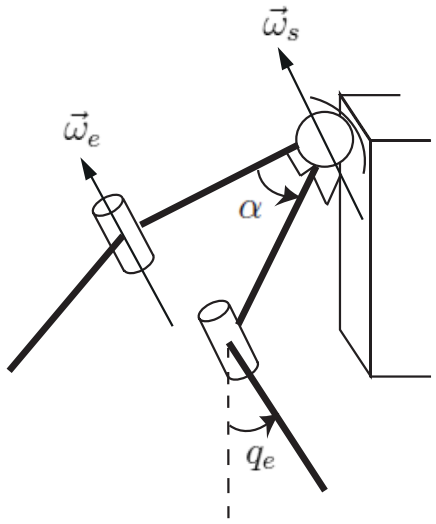

Figure 4. Rotation of the shoulder joint: α is the rotation angle for the shoulder joint about $\vec{\omega}_s$, q_e is the rotation angle for the elbow joint.

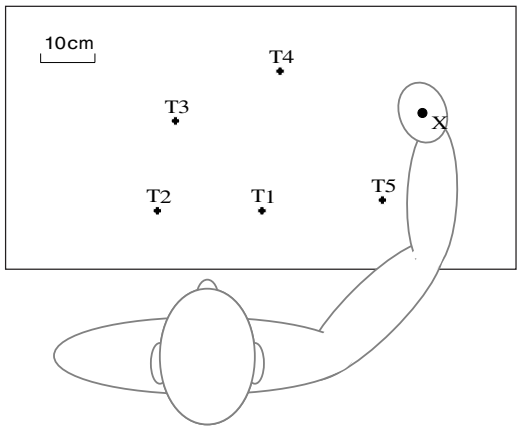

Figure 5. Initial and target positions.

The objective function remains the same as equation (12), where $D = \mathrm{Diag}\{d_1, \ldots, d_{2n}\}$. Setting

$$H = \sum_{i=1}^{n} V_i q_{n+i} + V_{n+i} u_i + \frac{\sigma_i}{2} V_{n+i,n+i} u_i^2, \quad (40)$$

from the necessary conditions $\frac{\partial H}{\partial u_i} = 0$, $i = 1, \ldots, n$, the optimal u_i^* are given by

$$u_i^* = -\frac{V_{n+i}}{\sigma_i V_{n+i,n+i}}, \; ; i = 1, \ldots, n. \quad (41)$$

The corresponding HJB equations are given by

$$-V_t = \inf_u \left[\sum_{i=1}^{n} V_i q_{n+i} - \frac{1}{2\sigma_i} \frac{V_{n+i}^2}{V_{n+i,n+i}} \right], \quad (42)$$

where V_i and $V_{i,i}$ respectively denote the first and second derivatives of V with respect to q_i. Assuming a solution $V(t, q)$ of the form

$$V(t, q) = k_0(t) + \sum_{i=1}^{n} k_{i1}(t) q_i^2 + k_{i2}(t) q_{n+i}^2 + k_{i3}(t) q_i + k_{i4}(t) q_{n+i} + k_{i5}(t) q_i q_{n+i}, \quad (43)$$

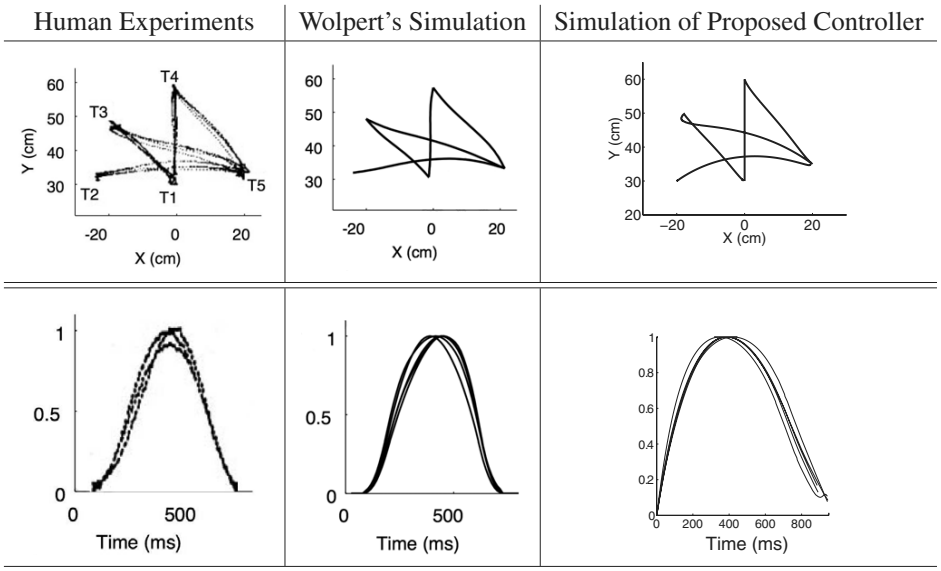

Figure 6. Comparison of proposed controller simulation results with Wolpert's simulation results and human experiment data. Upper figures show the hand space path. Lower figures show the tangential velocity profile.

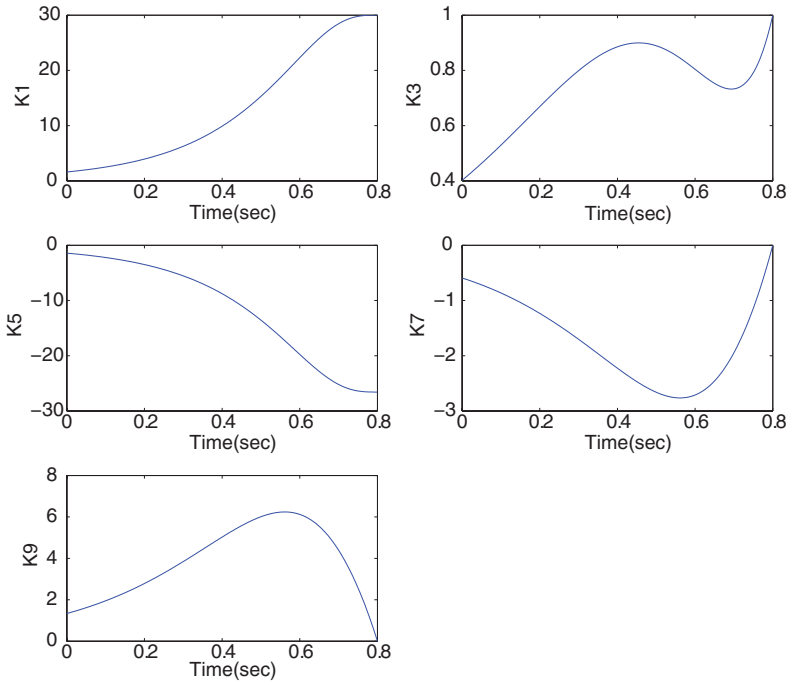

Figure 7. Feedback gain trajectories of movement $T_3 \rightarrow T_1$.

the optimal feedback controls u_i^* are of the form

$$u_i^* = -\frac{2k_{i2}q_{n+i} + k_{i4} + k_{i5}q_i}{2\sigma_i k_{i2}}, \quad i = 1, \ldots, n. \tag{44}$$

Since the feedback gains $k_{ij}(t)$ depend explicitly on t only, we obtain a set of ordinary differential equations for the gains as follows:

$$\dot{k}_{i1} = \frac{k_{i5}^2}{4\sigma_i k_{i2}} \tag{45}$$

$$\dot{k}_{i2} = -k_{i5} + \frac{k_{i2}}{\sigma_i} \tag{46}$$

$$\dot{k}_{i3} = \frac{k_{i4}k_{i5}}{2\sigma_i k_{i2}} \tag{47}$$

$$\dot{k}_{i4} = -k_{i3} + \frac{k_{i4}}{\sigma_i} \tag{48}$$

$$\dot{k}_{i5} = -2k_{i1} + \frac{k_{i5}}{\sigma_i} \tag{49}$$

$$\dot{k}_0 = \sum_{i=1}^{n} \frac{k_{i4}^2}{4\sigma_i k_{i2}}, \tag{50}$$

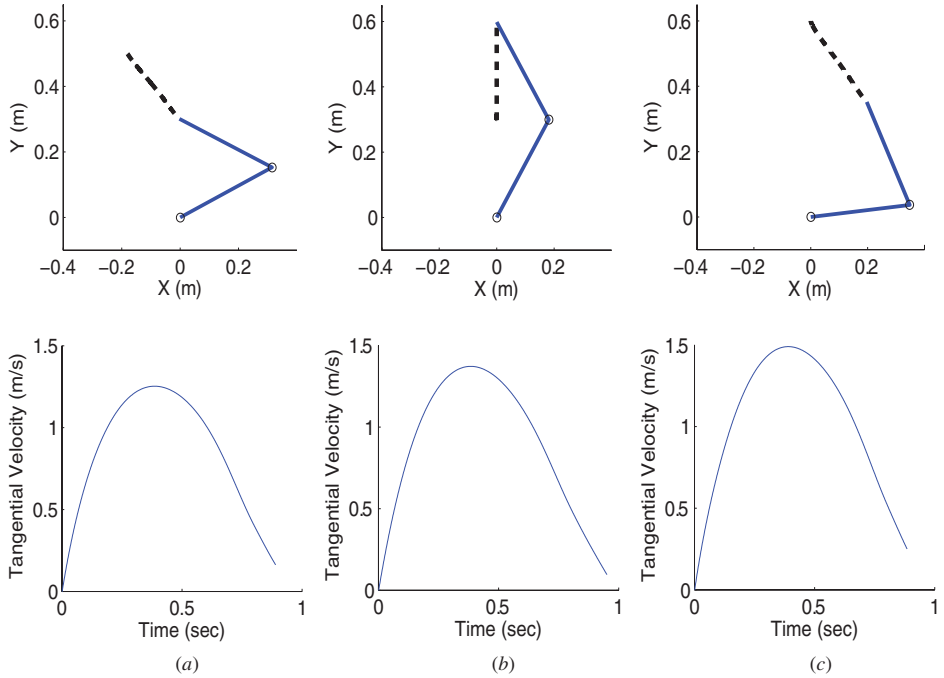

Figure 8. Optimal paths (dashed line) and their tangential velocity profiles. (*a*) $T_3 \rightarrow T_1$. (*b*) $T_1 \rightarrow T_4$. (*c*) $T_4 \rightarrow T_5$.

with the following boundary conditions:

$$k_{i1}(t_f) = d_i, \tag{51}$$

$$k_{i2}(t_f) = d_{n+i}, \tag{52}$$

$$k_{i3}(t_f) = -2d_i\bar{q}_i, \tag{53}$$

$$k_{i4}(t_f) = -2d_{n+i}\bar{q}_{n+i}, \tag{54}$$

$$k_{i5}(t_f) = 0, \tag{55}$$

$$k_0(t_f) = \bar{q}^T D\bar{q}, \tag{56}$$

for $i = 1, \ldots, n$.

Like the two-link planar chain case, appropriate values for the variance scale parameters σ_i need to be chosen according to the initial and goal postures. The procedure for the two-link planar chain does not directly generalize to arms with higher degrees of freedom. We therefore propose an alternative method of choosing σ_i values for the seven-DOF human-like arm of figure 10, that makes use of our earlier planar chain results of figure 3.

Since the three wrist joints have minimal effect on the overall arm motion, we consider the motion of the shoulder and elbow joints only. Given initial and final configurations of the arm, the proximal link in the initial configuration is assumed rotated by an angle α about the $\vec{\omega}_s$ to its final configuration (see figure 4). The unit vector $\vec{\omega}_e$ is assumed to be the rotation axis for the elbow joint. We first determine $\vec{\omega}_s$ and α, with α restricted to $[0, \pi]$. If the inner product of $\vec{\omega}_s$ and $\vec{\omega}_e$ of initial configuration is positive, q_s is set to α; if negative, q_s is set to $-\alpha$. q_s as obtained is then identified with q_1 of the two-DOF planar chain at the goal configuration (the initial value of q_s is, like that for q_1, zero). The initial and final values for the elbow joint q_e are further identified with the initial and final values for the planar chain elbow joint q_2, respectively.

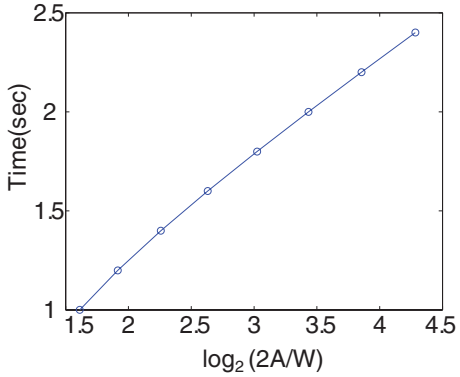

Figure 9. Movement time required to satisfy desired end-point accuracy.

Once initial and final values for q_s and q_e are obtained, the heading angle in joint space is determined, and values for the variance scale factors σ_s and σ_e are derived from the planar chain results of figure 3. Given σ_s, we then determine, among the three shoulder joint axes in the initial configuration, the one that is closest to $\vec{\omega}_s$ in a least norm sense; label this joint axis m. σ_m is then set to σ_s, while the σ_i for the remaining six joints are set to σ_e.

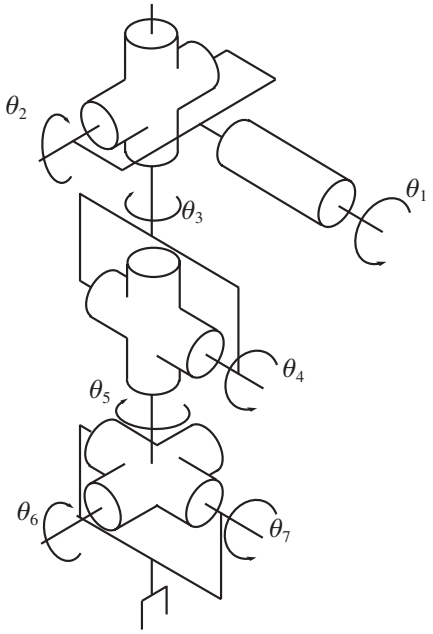

Figure 10. The seven-DOF robot arm used in the experiments.

The approach outlined is intuitively simple and computationally straightforward, and can be viewed as a first-order approximation of the four-DOF shoulder–elbow joint arm by a two-DOF planar arm. Of course, there are alternative, more sophisticated ways of making this approximation.

4. Experimental results

Numerical experiments are performed to evaluate whether the motions generated by our feedback control law resemble human arm movements (i.e., straight line hand trajectories, bell-shaped velocity profiles, Fitts law). Results for the two-link planar chain are first presented, followed by results for a seven-DOF spatial arm.

4.1. Two-link planar open chain

For the two-link planar chain, we follow the experimental procedure described in Flash and Hogan (1985): referring to figure 5, we consider the five movements $T_2 \rightarrow T_5$, $T_5 \rightarrow T_3$, $T_3 \rightarrow T_1$, $T_1 \rightarrow T_4$, and $T_4 \rightarrow T_5$. The results of human experiments are also presented in Flash and Hogan (1985) and reproduced in the left part of figure 6. To compare these with the hand paths generated by our feedback control law, like (Harris and Wolpert 1998) we also introduce a post-movement settling time phase—for our experiments the movement duration is set to 0.8 s, while the post-movement settling time was set to about 0.3 s, with a simple finite-time control law applied during the post-movement phase that results in the following error dynamics:

$$\dot{e} = a(1 - (e - b)^2), \tag{57}$$

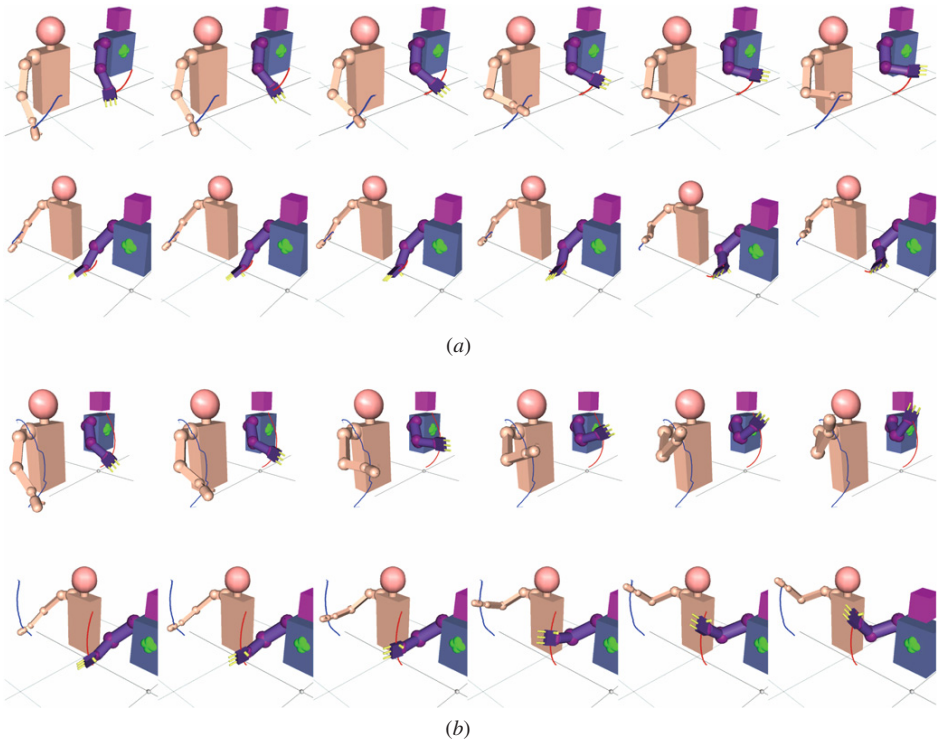

(*a*)

(*b*)

Figure 11. A frame-by-frame comparison of motions generated by our optimal feedback control law with human motion capture data: The pink arm represents the human arm, the purple arm represents the seven-DOF robot arm. The path traced by the robot end-effector is indicated in red. (*a*) Motion 1. (*b*) Motion 2.

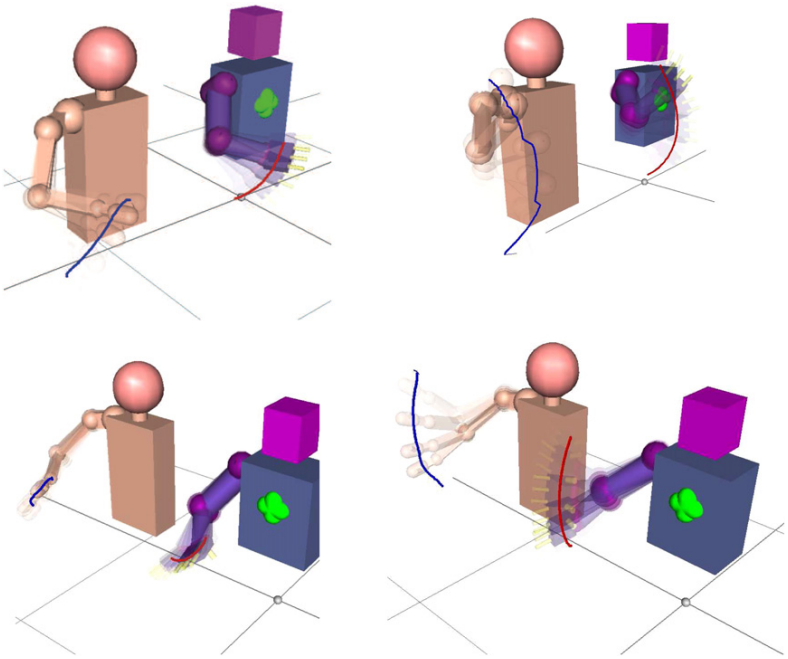

(*a*) (*b*)

Figure 12. End-effector trajectory comparison of motions generated by our feedback control law (red line) with human motion capture data (blue line). (*a*) Motion 1. (*b*) Motion 2.

where a and b are chosen to smoothly interpolate the trajectories during the transition of the controller, and respectively determined from the acceleration and velocity at the final time. This controller is designed to drive the error to zero while following the tangent hyperbolic function, i.e., $e = \tanh(a(t - t_f)) + b$. By setting $\dot{e}$ to u and e to $\dot{q}$, the joint velocity goes to zero smoothly and in finite time. Since $\frac{\mathrm{d}\dot{q}}{\mathrm{d}t} = u$, the corresponding state equations assume the form

$$\frac{\mathrm{d}\dot{q}}{\mathrm{d}t} = u = a(1 - (\dot{q} - b)^2). \tag{58}$$

Note that other finite-time controllers can be used, e.g., Haimo (1986).

Figure 7 shows the solution of equation (20) for movement $T_3 \rightarrow T_1$. Gain trajectories of other movements are similar in shape and we see that the gains are bounded and well-behaved.

Figure 8 depicts in more detail the optimal hand paths (figures in top row) and corresponding tangential speed profiles (figures in bottom row) for each of the three cases. Observe that these hand paths are linear like those of human trials, and the tangential velocity profiles are also bell-shaped as desired.

Figure 9 illustrates the extent to which our optimal trajectories satisfy Fitts Law, which was discussed earlier in section 1 and captured by equation (1). In our simulation, W is defined to be the error between the target and final position, and A the distance from the initial to the target position. The arm performs the same motion but subject to different movement times, and the positioning error at the final time is recorded. As predicted by equation (1), a linear relationship can also be found between task difficulty and movement time.

4.2. Seven-DOF spatial open chain

We now present results obtained with a seven-DOF robot arm (figure 10) with a kinematic structure and dimensions similar to that of the human arm. Trajectories generated by our feedback control law are compared with human arm motions obtained from motion capture data[2]. The initial and final postures for the robot arm, and also the movement duration, are set to match the motion capture data.

A frame-by-frame comparison of the generated and captured motions are shown in figure 11 for two representative arm reaching motions. The pink arm represents the captured human arm motion, while the purple arm represents the robot arm motion. We also compare the trajectories of the shoulder and elbow joint values (q_1, q_2, q_3, q_4) of the motion generated by our controller with the motion capture data in figure 13 (the inverse kinematics for the human subject is solved to obtain the measured joint trajectories). The close similarity between the two arm motions is immediately evident. Moreover, the path traced by the robot end-effector (indicated in red) is close to the path traced by the human hand (indicated in blue) as shown in figure 12. The tangential speed profiles (figure 14(*a*)) are also bell-shaped. The graph showing adherence to Fitts Law (i.e., the inherent trade-off between move duration and accuracy) is shown in figure 14(*b*); as desired, movement duration times increase proportionally to greater accuracy requirements.

[2] Courtesy Sensory-Motor Intelligence Laboratory, University of Texas at Arlington.

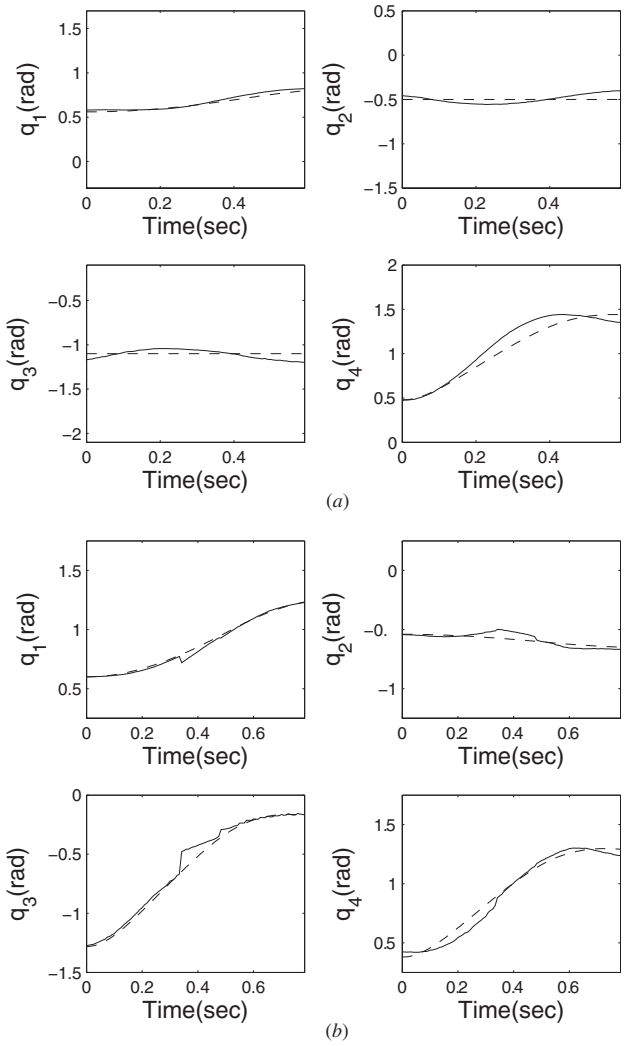

Figure 13. Joint trajectory comparison of motions generated by our feedback control law (dashed line) with human motion capture data (solid line). (*a*) Motion 1. (*b*) Motion 2.

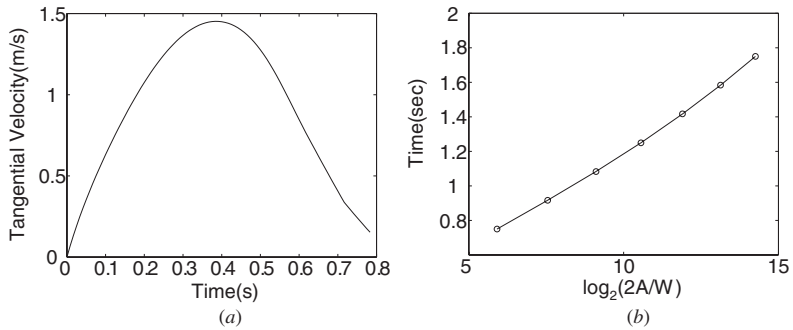

Figure 14. Features of robot arm trajectories generated by our optimal feedback control law. (*a*) Tangential speed profile. (*b*) Movement duration versus accuracy

5. Conclusion

In this paper we have proposed a stochastic optimal feedback control law for generating natural robot arm motions. Our approach is inspired by the minimum variance principle of Harris and Wolpert (1998) and the optimal feedback control principles put forth by Todorov and Jordan (2002) for explaining human movements. A crucial difference in our approach is that, by minimizing the endpoint variance in joint space rather than Cartesian hand space as done in Harris and

Wolpert (1998), not only are the resulting motions very similar to those of human arm movements, but the feedback control law generating the motions can be easily obtained in analytic form, by backward integration of a set of ordinary differential equations. In contrast to previous approaches, we show that it is enough to consider only the second-order kinematics—the dynamics are not included in the state equations—and that exact solutions to the nonlinear problem can be obtained rather easily; no linear–quadratic approximations are made at any stage of our algorithm, for example. The only parameters to be determined *a priori* are the variance scale factors; for both the two-DOF planar arm and the seven-DOF spatial arm, we offer a reasonably simple and intuitive method of setting these values based on experimentally obtained data.

Experiments have been conducted with a two-link planar chain and a spatial seven-DOF robot arm, whose kinematic structure and dimensions are similar to those of a human arm. Our results verify that the trajectories generated by our feedback control law closely resemble human arm motions, and appear to reasonably capture the essential features of human arm movements (nearly straight-line hand trajectories, bell-shaped velocity profiles, satisfaction of Fitts Law). Because the optimal feedback gains can be pre-computed offline, and nearly in real-time if necessary, our method offers a fast and convenient way of generating natural robot arm trajectories directly via a feedback control law.

Although it is not our intent to make any claims regarding the motor control mechanisms by which humans generate arm movements, our results nevertheless reinforce certain principles and also imply other possible explanations. First, our results to some extent reaffirm the validity of the minimum variance principle (Harris and Wolpert 1998) and the framework of stochastic optimal feedback control as the underlying mechanism for human motor coordination (Todorov and Jordan 2002), (Diedrichsen *et al* 2010). It may even offer a way to reconcile motor control theories based on the equilibrium point hypothesis (which, loosely speaking, rely on potential field-based feedback laws; see (Gomi and Kawato 1996) for a critique of some of its flaws) with optimal control principles like the minimum variance principle.

One departure from the minimum variance principle as stated in its original form is that motion generation may take place in internal (joint space) coordinates rather than external (task, or hand in the case of arms) coordinates. One common theory of voluntary human arm movements suggests that a high-level controller generates an optimal trajectory in hand space, and that a low-level controller then generates the joint trajectories required to track the given hand trajectory. It has been pointed out that such a dichotomy between high- and low-level control is unnatural, since it would imply, e.g., that the internal mechanical properties of the arm are not considered when generating the desired task space trajectory (Uno *et al* 1989); rather, any optimization is undertaken in internal (joint space) coordinates. Todorov (2004) also points out that a number of task coordinate-based optimality principles for explaining voluntary human movements (Flash and Hogan 1985, Meyer *et al* 1988, Harris and Wolpert 1998) do not take into account how the low-level controller operates. Other works have also made the similar argument that human motion optimization in joint space is more natural and effective (Kim *et al* 2006).

A second point of departure from Harris and Wolpert (1998) is that, at least for the case of simple arm reaching movements without any external loads, it is sufficient to only consider the second-order kinematics (that is, up to joint accelerations); internal models of the dynamics may not be necessary. Clearly further experimental verification of some of these ideas is necessary.

Acknowledgments

This research was supported in part by the Biomimetic Robotics Research Center, Center for Advanced Intelligent Manipulation, SNU-IAMD, and the BK21+ Program in Mechanical Engineering at SNU.

References

Arikan O and Forsyth D A 2002 *ACM Trans. Graph.* **21** 483–90
Diedrichsen J, Shadmehr R and Ivry R B 2010 *Trends Cogn. Sci.* **14** 31–39
Feldman A 1966 *Biophysics* **11** 565–78
Fitts P 1954 *J. Exp. Psychol.* **47** 381
Flash T 1987 *Biol. Cybern.* **57** 257–74
Flash T and Hogan N 1985 *J. Neurosci.* **5** 1688–703
Gabriel D A 1997 *Exp. Brain Res.* **116** 359–66
Gomi H and Kawato M 1996 *Science* **272** 117–20
Haimo V T 1986 *SIAM J. Control Optim.* **24** 760–70
Harada K, Hauser K, Bretl T and Latombe J C 2006 *Proc. IEEE Int. Conf. Robots and Systems* pp 833–8
Harris C M and Wolpert D M 1998 *Nature* **394** 780–4
Hinder M and Milner T 2003 *J. Physiol.* **549** 953–63
Khatib O 1986 *Int. J. Robot. Res.* **5** 90–98
Kim J H, Abdel-Malek K, Yang J and Marler R T 2006 *Int. J. Human Factors Modelling Simul.* **1** 69–94
Lim B, Ra S and Park F C 2005 *Proc. IEEE Int. Conf. Robotics and Automation* pp 4630–5
Meyer D, Abrams R, Kornblum S, Wright C and Smith J 1988 *Psychol. Rev.* **95** 1–31
Pollard N S, Hodgins J K, Riley M J and Atkeson C G 2002 *Proc. IEEE Conf. Robot. Autom.* **2** 1390–7
Ren L, Patrick A, Efros A, Hodgins J and Rehg J 2005 *ACM Trans. Graph.* **24** 1090–7
Seierstad A 2008 *Stochastic Control in Discrete and Continuous Time* (Berlin: Springer)
Shadmehr R 2003 *Handbook of Brain Theory and Neural Networks* ed M A Arbib (Cambridge, MA: MIT Press) pp 409–12
Simmons G and Demiris Y 2005 *J. Robot. Syst.* **22** 677–90
Todorov E 2004 *Nature Neurosci.* **7** 907–15
Todorov E and Jordan M I 2002 *Nature Neurosci.* **5** 1226–35
Uno Y, Kawato M and Suzuki R 1989 *Biol. Cybern.* **61** 89–101
Yamane K, Anderson S and Hodgins J 2010 *Proc. IEEE-RAS Int. Conf. Humanoid Robots* pp 504–10